

X-ray absorption spectroscopy of laser-produced plasmas: A study of the experiment and data analysis

J. Balmer

Institute for Applied Physics, University of Berne, Berne, Switzerland

C. L. S. Lewis, R. E. Corbett, E. Robertson, S. Saadat, and D. O'Neill
Department of Physics, Queen's University, Belfast BT7 1NN, Northern Ireland

J. D. Kilkenny, C. A. Back, and R. W. Lee

L-473 Lawrence Livermore National Laboratory, Livermore, California 94550

(Received 13 January 1989)

The novel technique of point-projection backlighting is used to probe a laser-produced plasma. A spatially restricted source of x rays is created by irradiating a fiber which is used to backlight a plasma. Temporal resolution of the absorption spectrum is obtained by creating the backlight with a pulse that is delayed in time from the main, plasma-producing, laser. The backlight can also be of shorter duration than the main laser pulse providing for enhanced time resolution and therefore less temporal averaging. The results for low- Z aluminum and silicon targets are presented. The low- Z absorption spectra using both low- Z (e.g., aluminum) and high- Z (e.g., molybdenum) elements for backlighting are studied. A description of this technique and the analysis of the data obtained is presented.

I. INTRODUCTION

The spectroscopic study of laser-produced plasmas is one of the most fruitful methods used to determine plasma parameters and ion level populations.¹ The more recent studies of, e.g., the soft x-ray-laser generating plasmas, have attempted to determine the spatial and temporal dependence of the detailed level populations in addition to the more common desire to obtain the temperature and density of the system. These studies have been successful insofar as they have provided more information about the plasma than was previously known. However, there is still a wide gulf between the predictions from detailed simulations of these systems and experimental observations.¹ There have been many possible explanations for this lack of agreement, such as experimental imperfections, e.g., laser nonuniformities in time and/or space, as well as difficulties in the theoretical development of the problem. In the latter category we have nonlocal heat conduction,² inadequate kinetics models,³ radiative-transfer effects,⁴ and the turbulence and instabilities effects that can arise in these laser-produced plasmas.⁵

A goal for the experimenters is to provide information on the plasma that will assist in understanding the plasma formation, dynamics, and kinetics *without* recourse to simulation, so that one may obtain enough information to define the problem completely. If this goal could be attained the simulations could be tested against the independently determined plasma parameters, ideally as a function of time and space. In the recent past, experimental improvements have centered on the improvements in diagnostic capabilities, which can now provide

time resolution on the order of ~ 50 ps for x-ray crystal streak cameras and ~ 150 ps for framing cameras,⁶ while for spatial resolution we have reached the level of < 10 μm with microscopes.⁷ However, emphasis so far has been on emission spectroscopy and an inherent problem is that the observations are strongly biased towards the large-oscillator-strength transitions from the upper-state populations of the prevalent ion species. This problem is generic to emission studies, which suffer from an inability to access the ionization balance directly since the overwhelming part of the populations are in the ground states. In fact, the ionization balance is of central importance to the study of the kinetics, which in turn is crucial to the prediction of x-ray-laser gain and is also a determinant of the temperature in the plasma. Thus the probing of the lower-level populations is of fundamental interest.

The difficulty with the development of the absorption techniques is that one is faced with an added diagnostic problem—the production and calibration of the x-ray source that is to be absorbed, i.e., the backlight. This difficulty has been alleviated recently by the work on the characterization of the laser-produced x-ray sources and specifically by the production of well-characterized small sources of x rays.⁸ This development naturally leads to the work presented here. In this paper we illustrate the first steps in the creation of an absorption technique that will provide a new level of information for the study and simulation of laser-produced plasmas.

The diagnostic technique employs a point x-ray-emitting plasma source that probes by projection a second larger plasma. This second plasma, the main plasma, absorbs the point-projected x-rays, which are then

reflected off a flat crystal. The recorded spectrum shows a source and absorption spectrum allowing a measurement of the population density of absorbing ion species in the main plasma with a one-dimensional spatial resolution of $\leq 10 \mu\text{m}$. The source brightness of a point source formed from *M*-shell emitters (e.g., Yb) irradiated by a short-duration-delayed laser pulse is adequate to record the motion of the expanding coronal plasma to ≤ 100 ps in the absorption spectrum. We also find that spectral resolution ~ 12.0 eV at photon energies in the range between 2 and 3 keV is possible.

In the following we will describe the experimental setup in Sec. II and review the results of the experiments in Sec. III. The data, which have an amalgam of backlight, self-emission, and absorption spectra on each laser shot, must be carefully analyzed. This analysis, which requires modest image processing, is discussed in Sec. IV together with the presentation of the reduced data. Finally, in Sec. V, a discussion of the experimental method and the next step toward implementation and improvement of the technique is given.

II. EXPERIMENTAL DESCRIPTION

The experiments described here were performed at the VULCAN laser at the Rutherford Appleton Laboratory and at the JANUS laser at Lawrence Livermore National Laboratory. The lasers were Nd glass operating at $2\omega_0$. The laser diagnostics provided the beam energies, the pulse duration, and the temporal histories. Two independent oscillators were used to generate different backlight

and main-plasma pulse lengths.

The schematic of the experiment is illustrated in Fig. 1. In the figure, the target material of interest initially forms a target in the shape of a foil, which is typically a $5 \times 1\text{-mm}^2$ slab with a thickness of $50 \mu\text{m}$. The target is made of plastic (Mylar) coated with the appropriate material. This target is irradiated by the main laser pulse on the $5 \times 1\text{-mm}^2$ surface, and the resultant plasma blows off on one side. A second synchronized laser pulse of short duration irradiates a thin wire or a coated-fiber target of diameter typically between 10 and $20 \mu\text{m}$ at its end. The backlight point source is created by a 100- or 600-ps $2\omega_0$ pulse of about 20 J focused to about a $30\text{-}\mu\text{m}$ spot, irradiating 10- to $20\text{-}\mu\text{m}$ fibers. The pins are typically made of tungsten wires $15 \mu\text{m}$ in diameter or $8\text{-}\mu\text{m}$ -diam carbon fibers built up to $15 \mu\text{m}$ diameter by plastic (CH) coating with a final layer of $0.5\text{-}\mu\text{m}$ -thick ytterbium. The quasicontinuous *M*-band emission from these high-*Z* backlights is suitable for use as an absorption source for the low-*Z* *K*-shell absorbing ions, as the $3d\text{-}4f$ transition bands of Yb were chosen because these coincide with the *K* absorption lines of aluminum.⁹ The resultant quasi-point-source plasma backlights the main plasma by projection. X rays from the backlight can propagate on both sides of the foil target before Bragg reflecting from a plane crystal and are finally detected on Kodak DEF x-ray film. Each different wavelength detected at the film plane has followed a slightly different path through the main surface plasma. All the detected wavelengths probe all the distances in front of and behind the foil target, limited only by the spectrometer entrance aperture. Typically a 1-ns or 600-ps $2\omega_0$ pulse at approximately 10^{12} W/cm² irradiated a 1-mm-diam spot or a $1 \times 5\text{-mm}^2$ line

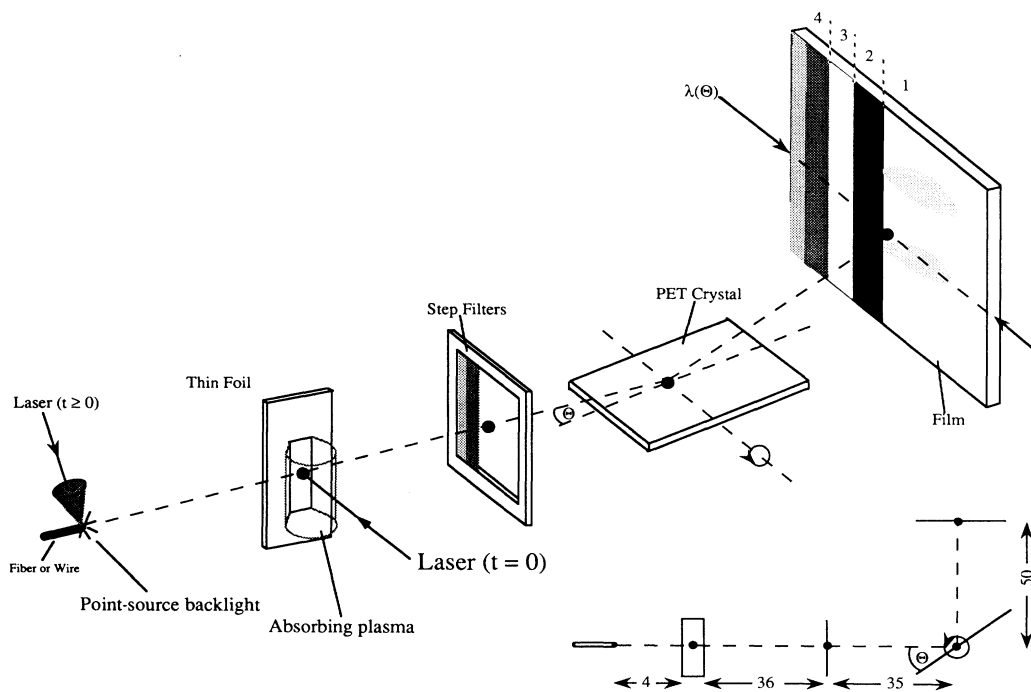


FIG. 1. Experimental setup and typical scale dimensions shown in millimeters. The regions imaged onto the film plane are discussed in the text.

on a foil of aluminum-coated Mylar to create the main plasma.

In the case of a *K*-shell backlight we have used an aluminum-slab target of dimension $250\ \mu\text{m}$ thick by $2\ \text{mm}$ wide which is irradiated by a 1-ns pulse of $\approx 12\ \text{J}$ at $1.06\ \mu\text{m}$ in a defocused spot of $1.0\ \text{mm}$ diameter. The resultant main plasma is probed by x rays emitted from a quasipoint backlighting source created by irradiating a $20\text{-}\mu\text{m}$ -diam aluminum wire with an 0.8-ns pulse of $\approx 15\ \text{J}$ at 2ω in a spot of $100\ \mu\text{m}$ diameter at the wire position. This arrangement provides the intense backlight emission in the spectral region of the surface plasma absorption.

The experimental arrangement in Fig. 1(b) illustrates that the projection magnification to the film plane, in both backlight cases, will be 31 times, with the two plasmas separated by $\approx 4\ \text{mm}$. Each part of the film provides four pieces of information on each shot and is recorded in regions 1–4, as indicated in Fig. 1(a), which covers an area of $40\times 30\ \text{mm}^2$. Region 1 records the absorption spectrum, superimposed on the line emission, over a spectral range typically from 4.5 to $7.5\ \text{\AA}$ for a pentaerythritol (PET) crystal. Region 2 is an edge-on shadow of the foil which provides a record of the background level on the film that is due to either the self-emission from the main plasma or fluorescence from the crystal and filters. Region 2 also provides an alignment check as the shadow width can be calculated from the geometry of the setup. Region 3 is the backlighting spectrum from behind the main foil and provides a record of the source spectrum, which can be divided into the backlighting spectrum to provide opacity data as a function of wavelength. Region 4 is a step-wedge filtered-source spectrum, typically made up of $25\ \mu\text{m}$ beryllium or $10\ \mu\text{m}$ melinex steps, which provides a film calibration at each wavelength. The filters are located along one edge of the spectrometer entrance aperture. The crystal can rotate so that a particular line seen in absorption and self-emission can be brought to the same position at the film plane. In this alignment the chosen wavelength probes the central portion of the main plasma.

The spatial resolution, which is central to the purpose of the experiment, was tested by backlighting a copper grid constructed of $30\text{-}\mu\text{m}$ -wide bars and a $120\text{-}\mu\text{m}$ period with a tungsten wire of $20\ \mu\text{m}$ diameter irradiated with a 600-ps laser pulse. In Fig. 2 the results of such a test are shown. In the regions where there is continuous emission the spatial resolution is better than $10\ \mu\text{m}$. Although the opaque wires are $30\ \mu\text{m}$ wide, the edge response was less than $10\ \mu\text{m}$. In regions of the spectrum where the line emission is strong the resolution is worse and in fact depends on the particular line. This indicates that the backlight-source plasma is effectively smaller for continuum emission than for the line emission, largely because the line emission is from a larger expanding plasma. This observation is supported by the x-ray crystal streak camera data, which shows the continuum emission closely following the laser-pulse history and the line emission generally lasting for long times. For spectral regions dominated by continuum the spectral resolution is largely determined by the crystal rocking curve and spatial resolution by the backlight-source size.

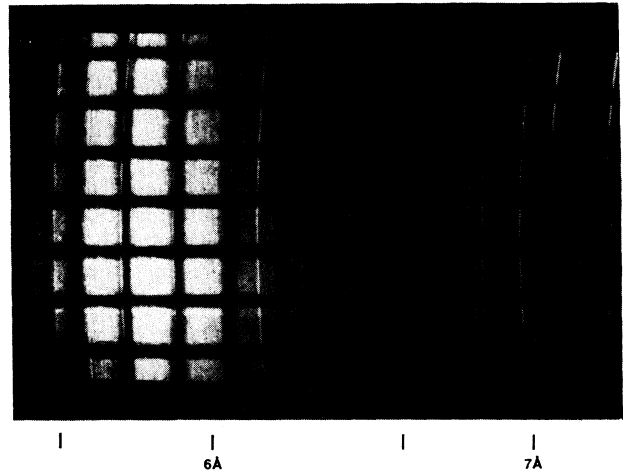


FIG. 2. Resolution grid showing the limitations on the spatial resolution due to source size and intensity. The source is a quasipoint tungsten pin. The grid has $30\text{-}\mu\text{m}$ -thick wires with a period of $120\ \mu\text{m}$.

III. EXPERIMENTAL RESULTS

The results obtained using the technique described in Sec. II are presented here. In this section we describe a number of experiments to illustrate that the high-*Z*, short-duration backlight is the appropriate combination for maximizing the information content. In Fig. 3(a) are the results for a shot with an aluminum main-surface plasma created by a $2\omega_0$, 8-J 1-ns pulse and backlit with an aluminum quasipoint source created by a 20-J pulse. The film record is shown after it has been converted from film density to intensity and this illustrates the four regions of the film as described in Sec. II, although the wedge does not reproduce well. The backlight is of 600 ps duration and therefore represents the time resolution of the absorption spectrum. The broad emission lines seen in the picture are from the surface plasma and present a difficulty in the interpretation of the data. However, the absorption lines can be readily observed as dark regions within the broad emission regions. The lines of the heliumlike series $1s^2-1snp\ ^1P$ can be observed up to the principal quantum number n equal to 6. This shot illustrates that aluminum backlighting aluminum has an advantage in the simple interpretation of the spectral features in absorption, which by necessity occurs where the emission occurs. The absorption signal must be obtained by subtracting the surface-plasma emission and then dividing the residual surface-plasma signal by the residual source spectrum. This source is obtained from the observed unattenuated backlight emission which passes behind the foil.

In Fig. 3(b) we see the results for an aluminum surface plasma created by a 22.0-J pulse backlit by a ytterbium plasma created by a 8.7-J pulse which had a duration of 100 ps. The time delay between the peak of the Gaussian main pulse and the peak of the backlight pulse was 0.0 ps. We can see in this figure that the intensity of the backlight is quasicontinuous across the spectral region of in-

terest but that it also has a spectral-line structure, i.e., it is not a pure continuum. This structure must be divided out of the observed spectrum to produce the correct absorption features in analysis similar to the spectrum in Fig. 3(a). Further, note that the Al emission, which is long lived and not imaged, partially illuminates the film plane in the shadow of the foil. There is improved resolution using the quasicontinuous source both temporally and spatially. The temporal resolution is due not only to the backlight duration for the shot in Fig. 3(a), which

yields a longer "frame" time, but also because the emission times for the aluminum *K*-shell resonance lines are much longer lived than the backlight-laser pulse. This has been observed in numerous experiments and is well documented.¹⁰ The decreased spatial resolution is due also to the longer-lived emission of the more intense lines, that is, the longer-lived lines emit from a larger spot. Since the spot size dictates the spatial resolution the aluminum backlight provides a larger effective spot. The result of the improved resolution can be illustrated by the

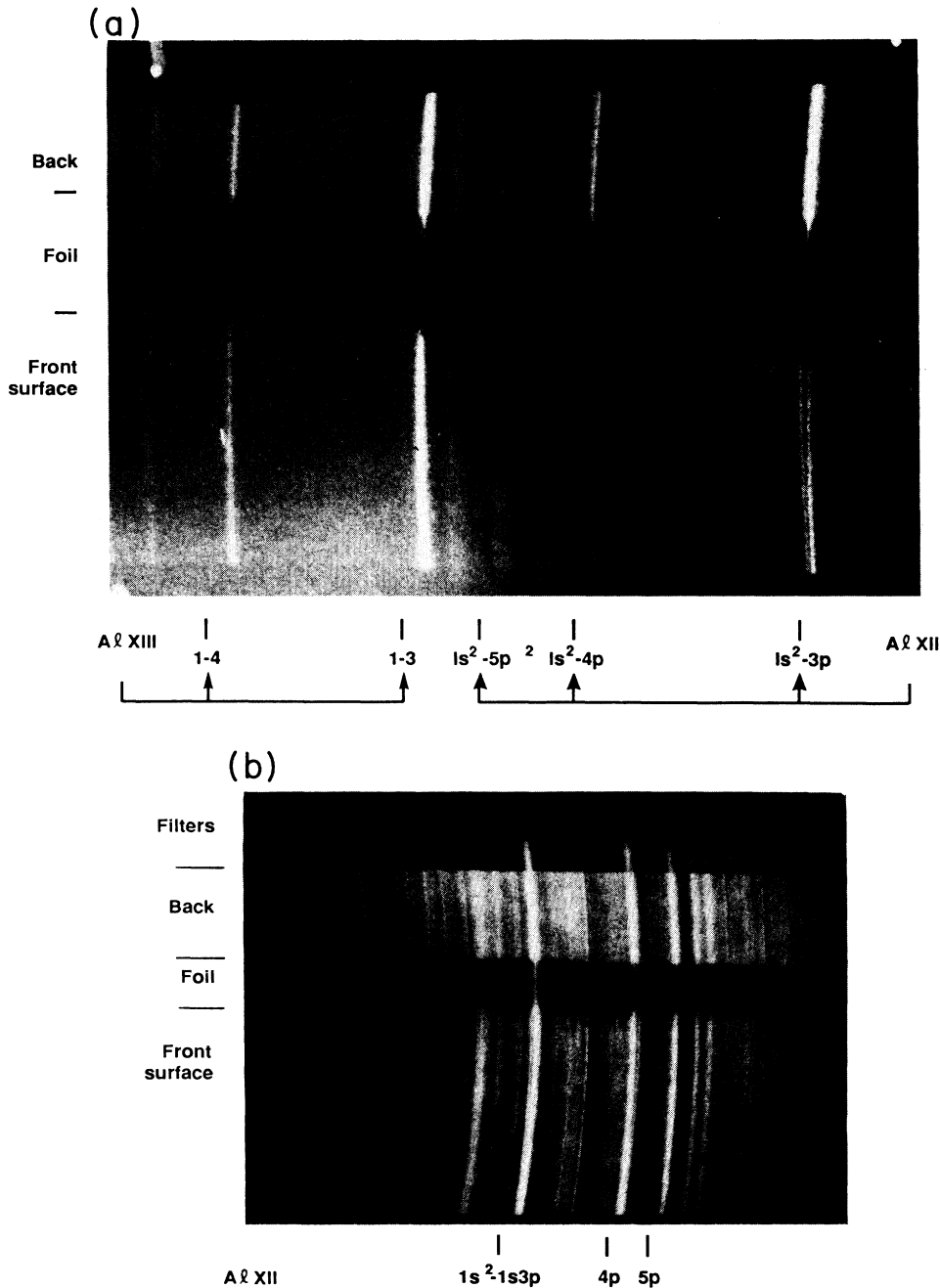


FIG. 3. (a) Data for an aluminum target backlit by an aluminum point source with a delay of 0 ps from the main pulse and a duration of 600 ps. (b) Data for an aluminum target backlit with a ytterbium point source with a delay of 0 ps from the main pulse and a duration of 100 ps.

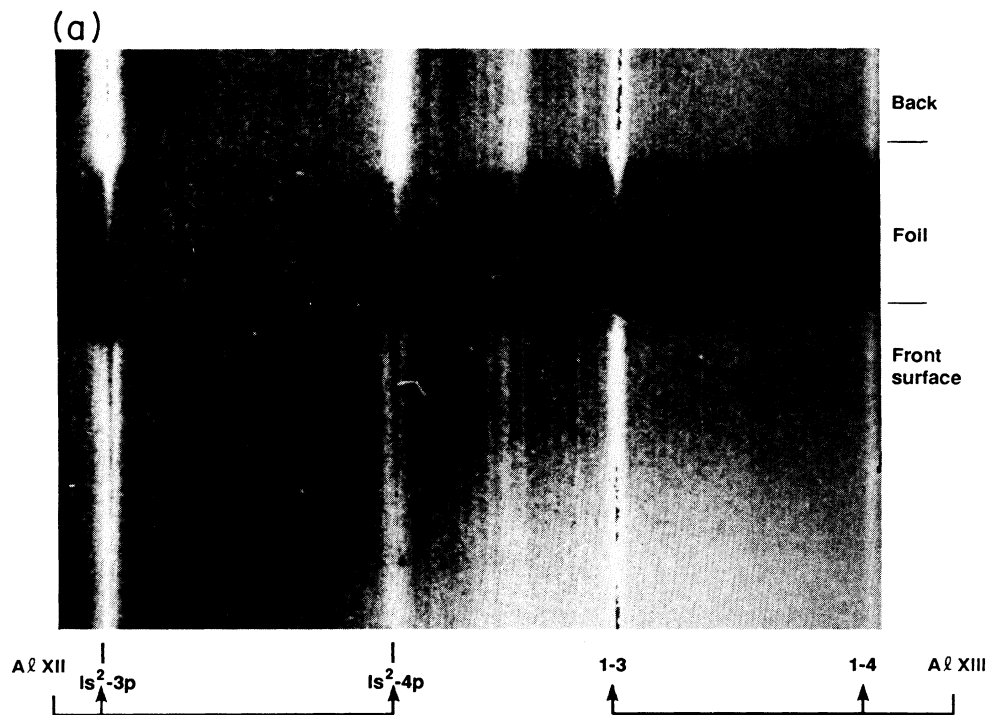


FIG. 4. (a) Processed data from shot illustrated in Fig. 3(a). (b) Processed data from an aluminum target backlit with a tungsten backlight of 600 ps in duration. Note that improved resolution is obtained with the broadband backlight source and that the complex structure of the backlight source is not a difficulty in the interpretation of the data.

observation of a number of satellite features associated with the resonance lines which are found close to the target to the target surface, i.e., $\leq 20 \mu\text{m}$ for the quasicontinuous backlight of 100 ps duration. Next, the film data were digitized using a Perkin-Elmer microdensitometer system. The digitized images are converted from density to intensity using a calibration step wedge. The data are then handled as a two-dimensional graphical image which is manipulated by image-processing software.

In Fig. 4(a) the processed data are produced for the aluminum surface plasma backlit by aluminum shown in Fig. 3(a). In Fig. 4(a) three processes have been performed to obtain the interpretable data shown. This processing is carried out using the image-processing code IMAGIC of Hansom. First the curvature of the spectrum has been removed by means of an elementary tracking algorithm which fits a quadratic to the tracked spectral features along the film. The curvature of the spectrum is then removed by using a low-order polynomial to interpolate the curvature in the spectral direction between the tracks. Second the self-emission of the surface must be subtracted from the image. To accomplish this we use the fact that the experimental setup does not have a slit in front of the spectrometer, so that the surface-plasma emission is not spatially resolved. Therefore, the emission observed in the region, which is the shadowed image of the side of the foil, is due entirely to the surface plasma. This region is sampled and the resultant spectrum is subtracted from the entire film. Finally, the third step is to determine the absorption source spectrum and divide

the image by this source. To determine the unattenuated absorption spectrum we sample the region behind the foil, i.e., on the unirradiated surface, and use this to divide the total image. The results of this processing are shown in Fig. 4(a). Note that the absorption spectrum is enhanced and that the limits of the processing can be seen in the introduction of some extraneous features where the subtraction and/or division results in the enhancement of the noise. Figure 4(b) shows processed data from an aluminum surface plasma that was irradiated by a 1-ns pulse and backlit by a tungsten plasma created by a 600-ps irradiation, which is delayed from the main surface-plasma laser by 250 ps. A comparison between the two experimental results in Fig. 4 shows that for the same backlight-pulse length, which implies the same frame time for the absorption, the improved resolution of the quasicontinuous source is clearly an advantage. Further, the image processing of the data renders the complex spectral character of the high-Z backlight unimportant in the final analysis of the data.

In Fig. 5 we present the processed data for the aluminum surface-plasma irradiation, backlit by an ytterbium plasma, as shown in Fig. 3(b). The time delay between the main-laser pulse and the backlight pulse is 0.0 ps. There are features in the spectrum that do not appear in the tungsten backlit spectrum shown in Fig. 4(b) because these features have been lost due to smearing inherent in the 600-ps frame time. The features are the numerous satellites of the heliumlike and hydrogenlike resonance lines that arise from the lithium-, beryllium-, boron-, and

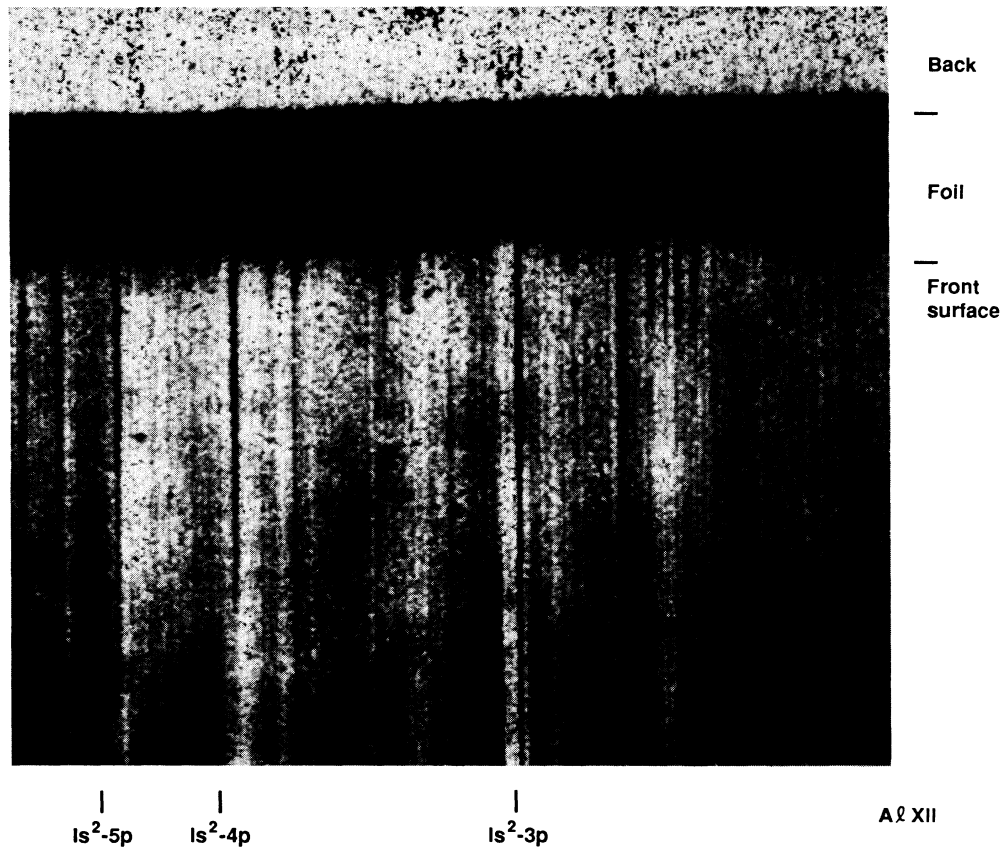


FIG. 5. Processed data from the experiment shown in Fig. 3(b).

the instrument resolution. In the current experiment the spectrometer resolution is defined by the rocking curve of the crystal. Assuming that this introduces a Gaussian instrument profile I_I we can determine the total observed profile I_O as a convolution of the instrument function and the intensity transmitted I_T

$$I_O(\nu) = \int I_T(\nu - \nu') I_I(\nu') d\nu' . \quad (2)$$

The crystal rocking curve is assumed to be Gaussian with a full width at half-maximum of $\Delta\nu_R$, which is determined to be $\approx 3 \times 10^{-4}$ rad for the PET crystal used. The value of $\Delta\nu_R$ was estimated from the clearly resolvable fine-structure splitting in the hydrogenic-aluminum Lyman- α transition, i.e., 5 mÅ at 7.2 Å.

Two possible methods of analysis are now presented. In the first we observe the transmission at a single frequency corresponding to the line center of one of the transitions in the heliumlike series, the $1s4p-1s^2$ line. This yields a transmission versus distance for a series of times. The reduction to ground-state number density is discussed. In the second method we look at the entire line series of the heliumlike aluminum and attempt to ascertain the density of electron and the ground-state population consistently. This method is similar in spirit to the curve of growth methods that are used in the analysis of stellar spectra. This latter method is more

complex but may lend itself to analysis of the absorption data without recourse to detailed simulation, which would be an advantage if testing the simulation capability is one of the desired goals of the experiment.

A. Line-center transmission analysis

Using the film calibration, the source, and the absorbed spectrum intensities, which are above the background, an opacity at the line-center position τ_0 for each line can be measured for all observed transitions at various distances z from the target surface. These measured opacities are the corresponding optical depths that are averaged over the frame time. With the knowledge of the absorption path length l , which we obtain from the pinhole camera images, an estimate can be made of the ground-state ion density N_g at each distance from the target surface. This simple procedure assumes that the spectral line width is well resolved and can be measured. In the current experimental setup we have an instrumental profile that is well characterized but nonetheless reduces our sensitivity to the optical depth at any point on the profile. That is, the measured transmission at line center is no longer given by $\exp(-\tau_{v_0})$ but by a convolution of the true transmission and the instrument function. Thus, the observed transmission at line center is given by

$$T_{\nu_0}^{\text{obs}} = (1/\Delta\nu_R) \int d\nu \exp(-\tau_\nu) \\ \times \exp\{-4 \ln(2)[(\nu_0 - \nu)/\Delta\nu_R]^2\},$$

where $\Delta\nu_R$ is the full width at half-maximum due to the spectral resolution of the crystal. It is clear from the equation that if the ratio of the width due to the instrument resolution to the intrinsic width, assumed to be the Doppler width Δ_D , which characterizes τ_ν , is small, then the observed transmission is equivalent to the undegraded transmission. However, in the present case we have a ratio of $\Delta_R/\Delta_D \approx 1.7$, which means that for low transmission, i.e., on the order of 0.3 or less, the broadening due to the instrument becomes dominant. Thus we must restrict the analysis to those regions where the transmission is 0.3 or greater, i.e., the regions of lower density. This integral can be rewritten to illustrate the dependencies more clearly:

$$T(\nu_0) = (1/\Delta\sqrt{\pi}) \int dx \exp[-\tau_0 \exp(-x^2)] \\ \times \exp(-x^2/\Delta^2),$$

where

$$\tau_0 = 1.53 \times 10^{-16} f N_g l \lambda_0 \sqrt{Z/T_{ev}}, \\ \Delta = \Delta_R/\Delta_D \approx 4.69 \sqrt{Z/T_{ev}}.$$

The relationship of the intrinsic linewidth to the instrument width and its effect on the observed transmission are shown in Fig. 6(a) for the case where Doppler effect is the dominant line-broadening process. In the figure the observed transmission is presented for various values of the optical depth at line center. Note that the critical relationship is the ratio Δ_R/Δ_D and this indicates that the curve is a function of the temperature. Thus in Fig. 6(a) there are different curves for each temperature. This indicates that we must ascertain from the data both the ground-state number density and the temperature consistently. The data available from the experiment provide the type of information necessary for the consistent solution of the parameters, since there are numerous lines from the same ground state which differ only in oscillator strength and wavelength, both of which are well known. Thus we can analyze the data from the experiment.

In Fig. 6(b) the analysis of the $1s4p\ ^1P - 1s^2\ ^1S_0$ transition is shown for different time delays of the backlight pulse. The transmission at each time provides a mapping of the ground-state population of the heliumlike aluminum ion. The backlight in these experiments was 600 ps in duration and the surface plasma was produced using a 1-ns pulse of 1.06- μm light. Figure 6(b) illustrates the wealth of data obtained from the analysis. To reduce these data to number density we would make recourse to the fact that the other transitions from the same series are also observable, so that an independent measure of the plasma density could be obtained from the pressure-broadened line profiles. This together with the simplifying assumption that the observed plasma is isothermal would allow one to obtain a temperature by the following analysis. First, the electron density and the ion density are related by the equation

$$N_e/N_T = \sum_i Z_i N_i/N_T,$$

where N_i and N_T are the densities of the ionization stages and the total ion density, respectively. Second, information on the relative ionization balance from the spectra, i.e., the relative contributions of different ions, provides the quantities N_i/N_T , allowing us to solve for N_T . Third, the information on N_T provides the solution for the quantity of interest N_i . When this is done we could find a consistent set of temperature and ground-state populations for the plasma at each time. However, the problem of circumventing the instrument function creates an inherent difficulty and a loss of accuracy. Thus, it is of interest to use all the information available to us at the outset and not attempt to piece only a part of the complex plasma development together when the entire set of information will provide a better interpretation. The results of the analysis in Fig. 6(b) indicate the wealth of data that can be extracted from the experiment; however, to interpret this the entire absorption profile must be used.

B. Line series absorption technique

To analyze the data we have used line-center transmission to measure the optical depth and then related that to the opacity length product to infer the ground-state number density of the heliumlike aluminum ions. The difficulty with this technique is that we use a single point on the absorption profile and we are restricted in the information content by the fact that the instrument function degrades the original absorption data. The disadvantages inherent in the line-center transmission analysis can be circumvented by using the entire absorption line profile and integrating the area contained in the profile. By integrating over the entire curve we are using the fact that the absorbed energy should be a conserved quantity and that the instrument function will be integrated out. There is still an inherent loss of information when the instrument function degrades the signal such that the low transmission values are less accurate as the signal is influenced by the noise inherent to the plasma emission.

The integration of the absorption function over all frequencies in the profile is a well-documented technique in the astrophysical literature and the resulting dependence of the integrated absorption versus the $N_g l$ is referred to as the curve of growth. In the present case the integration of the absorption follows from the formula

$$W(N_g l) = \int_{-\infty}^{\infty} d\nu' (1 - T_{\nu'}^{\text{obs}}) \\ = \int_{-\infty}^{\infty} d\nu' \int_{-\infty}^{\infty} d\nu [1 - \exp(-\tau_\nu(N_g l))] \Phi(\nu' - \nu),$$

where the Φ is the instrument function, normalized so that the integral over frequency is unity, and W is defined to be the equivalent width for the particular $N_g l$ product. By interchanging the order of integration, we note that the equivalent width is the same as that obtained for the case where the instrument function does not affect the observation.

In the usual astrophysical case the curve of growth is

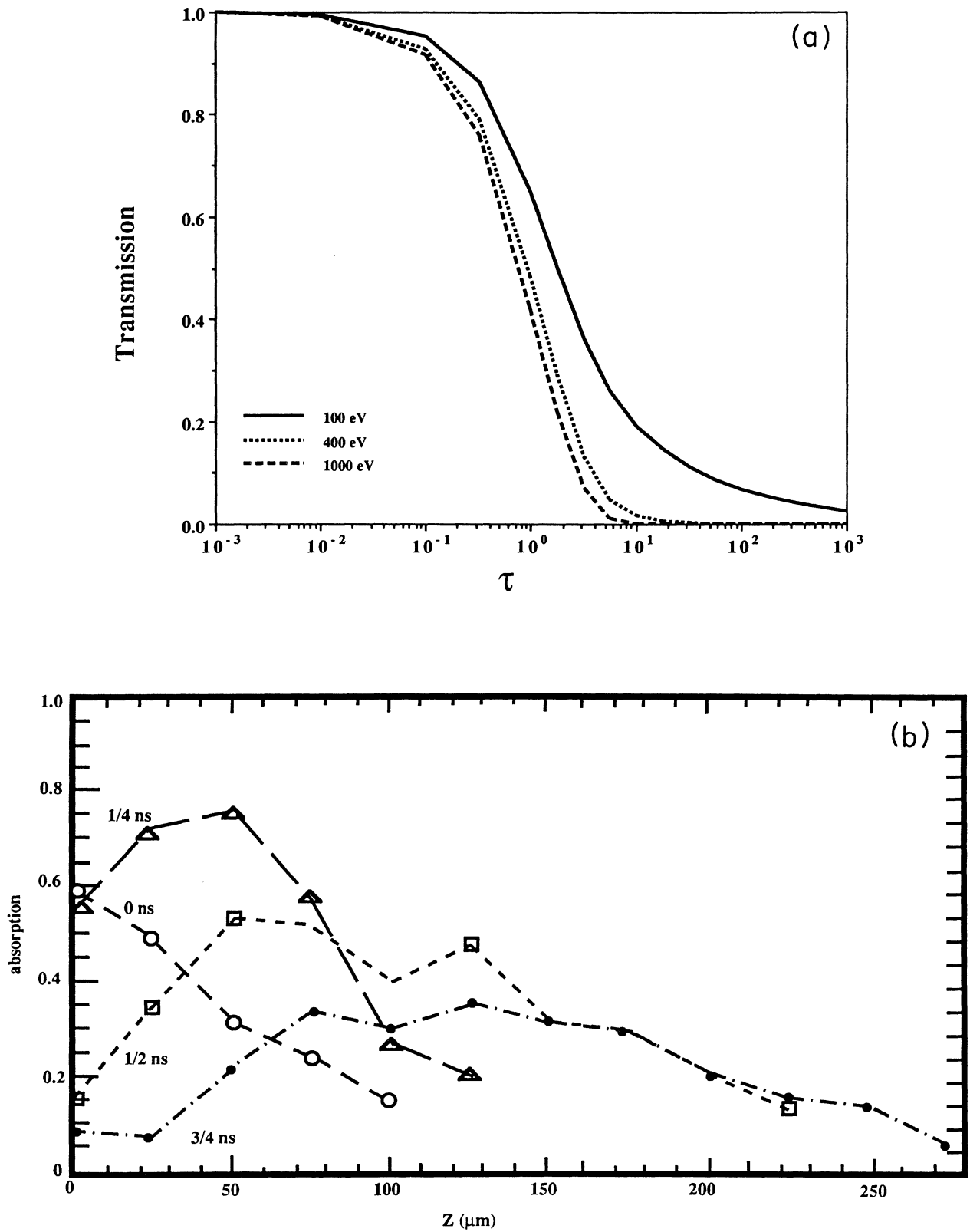


FIG. 6. (a) Observed transmission vs the optical depth for various values of the temperature. Note that the transmission depends on the temperature and the $N_g l$ product. (b) Results obtained by analyzing a series of experiments with different backlight delays. The backlight was 600 ps in duration. The curves at the different times represent the transmission vs the distance from the target surface measured in micrometers.

given for a Voigt-type line profile. In the core of the line the Doppler profile is dominant and the curve of growth has a well-defined slope for low optical depths that sample this region of the line profile. For large optical depths, when the transmission is dominated by the line wings, the ratio of the collisional to Doppler width of the line will dictate the slope of the curve of growth. In the present case we have the ability to better approximate the line-shape behavior by calculating the line profile using the Stark-broadening formalism and fitting the line-wing slope to the formula

$$I_{\Delta\nu}^{\text{asymptote}} \propto \Delta\nu^{-5/2} \exp(-\kappa\Delta\nu^{-1/2}),$$

where the value of κ is determined by empirically fitting the wings of the line profile. The formulation is rigorously correct for the Lyman- α line of neutral hydrogen, when there is only one Stark component in the composition of the line shape and the microfield varies as $\Delta\nu^{-5/2}$. However, in the case of He-like ion transitions complications arise from the exponential term which is not present for the case of neutral species. (Thus in the neutral emitter cases additional Stark components can be added and the linearity of the approximation scheme would be preserved.)

Within these constraints the curve of growth is calculated for the various line profiles that are observed in the experiments. In Fig. 7 we show the equivalent width in units of electron volts versus the $N_g l$ product. There is a set of curves for each line transition, denoted by β , γ , δ ,

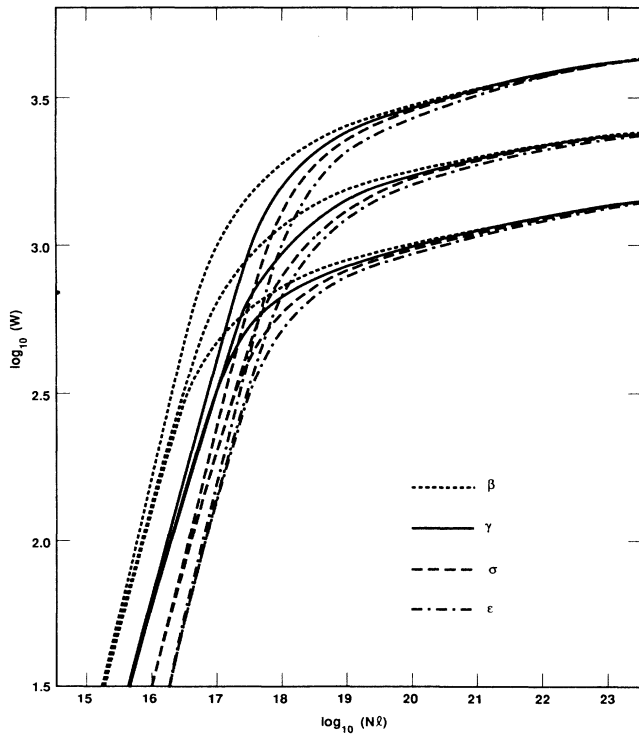


FIG. 7. Curve of growth for the Stark-broadened lines of the heliumlike resonance series. The units of the equivalent width W are in eV and the Nl is in cm^{-2} .

and ϵ for the transitions $1s^2^1S$ to $1snp^1P$ where $n=3,4,5,6$, for each of the three plasma temperatures 100, 300, and 1000 eV. These temperatures were chosen to bracket the observed results. The curves in Fig. 7 are dominated by the Doppler profile in the line core; hence at low $N_g l$, giving the same equivalent width for a transition at all temperatures. The high-optical-depth region of the curves is dominated by the asymptotic wings. The fact that we have numerous lines with the same $N_g l$ provides for an over specification of the problem and leads to the determination of the estimate of the $N_g l$ in Fig. 8. In Fig. 8 we show the equivalent width as a function of distance from the target surface for the experiment described above and shown in Fig. 5. In addition, the $N_g l$ product is shown along the abscissa. This $N_g l$ is determined by optimizing the fit for all lines at a particular plasma position for one temperature. The temperature is optimized at 250 eV with a variation of +100 and -50 eV. The results of this analysis indicate that the initial density gradient can be characterized by the present method.

V. DISCUSSION

We have shown how an experiment to measure the absorption spectrum of a laser-produced plasma can be analyzed to infer the ground-state population of the heliumlike ion species. In producing this information we are able to make estimates of the ionization balance and the temperature of the plasma as a function of time and space. This level of detail when coupled with the emission studies that have been perfected in the study of laser-produced plasmas provides a major step forward in producing basic data that could be used to interpret the plasma parameters without recourse to simulation or other detailed kinetic modeling schemes.

To improve the experimental design a number of

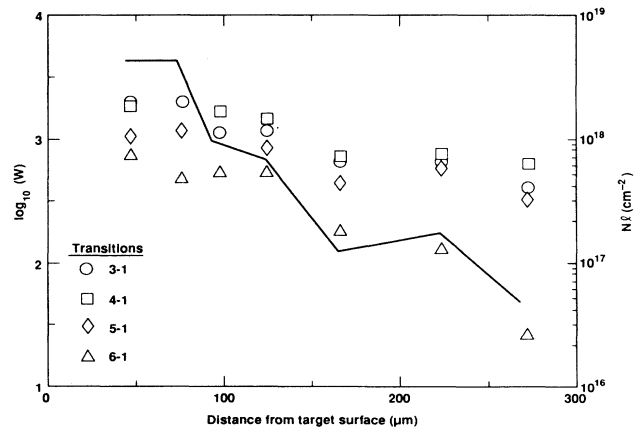


FIG. 8. Results of analyzing the experiment shown in Fig. 3(b). The equivalent width for each member of the He-like Al line series noted in Fig. 7 is shown as a function of distance from the target in micrometers. In addition, the $N_g l$ product that arises from the analysis of the equivalent widths, i.e., using Fig. 7, is also indicated. The temperature is determined to be ~ 250 eV.

modifications would be necessary. First, the gradients in the plasma could be reduced by fabricating a target with the material under investigation restricted in area as with spot spectroscopy. In this way the backlight could probe a smaller, more uniform region of plasma and thus limit the uncertainties in the absorption path length and gradients in the plasma. Second, the backlight-pulse duration should be made as short as possible so that the temporal averaging would be reduced. The improvements that can be obtained by reducing the backlight duration are observable by noting the differences in the spectrum taken with 600 versus 100-ps backlights, shown in Figs. 3 and 4, respectively. Finally, the choice of the target material can be modified so that we observe more complex spectra. In the present case the *K*-shell absorption is

shown and the number of distinct features that are analyzed is large but the individual features have much redundant information. In the future the use of high-*Z* species will be explored to determine the effectiveness of obtaining the ionization balance from an ion-producing absorption from the $n = 3$ shell.

In summary, we have presented the first absorption spectroscopy experiments on laser-produced plasmas where there is temporal and spatial information provided by the spectra independent of a simulation capability. This type of information is essential for the improvement of our understanding of the production of laser-produced plasmas and the development of new sources of plasmas for unique applications.

-
- ¹V. A. Boiko, A. Ya. Faenov, and S. A. Pikuz, *J. Quant. Spectrosc. Radiat. Transfer* **19**, 11 (1976); J. D. Kilkenny, R. W. Lee, M. H. Key, and J. Lunnery, *Phys. Rev. A* **22**, 2745 (1980).
- ²R. L. Kauffman, R. W. Lee, and K. G. Estabrook, *Phys. Rev. A* **35**, 4280 (1987); A. Hauer, O. Willi, J. D. Kilkenny, and C. Hooker, *Phys. Rev. Lett.* **52**, 2563 (1982).
- ³D. Duston and J. C. Davis, *Phys. Rev. A* **21**, 932 (1980); R. W. Lee, B. L. Whitten, and R. E. Strout II, *J. Quant. Spectrosc. Radiat. Transfer* **32**, 91 (1985).
- ⁴J. C. Apruzese, P. C. Kepple, K. G. Whitney, J. C. Davis, and D. Duston, *Phys. Rev. A* **24**, 1001 (1981); J. C. Salter, L. A. Yobs and R. W. Lee, *J. Quant. Spectrosc. Radiat. Transfer* **39**, 134 (1988).
- ⁵See C. E. Max, Lawrence Livermore National Laboratory, University of California Report No. UCRL 53107 1982, Vol. 1 (unpublished).
- ⁶J. Balmer, W. Lampart, E. Roschger, J. D. Hares, and J. D. Kilkenny, *Rev. Sci. Instrum.* **56**, 860 (1984).
- ⁷R. J. Ellis, J. D. Kilkenny, R. A. Levesque, D. W. Phillion, and D. J. Deane, University of California Report No. UCRL 96623, 1988 (unpublished).
- ⁸D. L. Matthews, E. M. Campbell, N. Ceglio, G. Hermes, R. L. Kauffman, L. Koppel, R. W. Lee, K. Manes, V. C. Rupert, V. W. Slivinsky, R. Turner, and F. Ze, *J. Appl. Phys.* **54**, 4260 (1982); B. Yaakobi, P. Bourke, R. McCrory, W. Seka, J. M. Soures, A. J. Burek, and R. Deslattes, *Opt. Commun.* **38**, 196 (1981).
- ⁹A. Zigler, R. W. Lee, J. D. Kilkenny, G. Kolbe, and H. Nathel, *J. Appl. Phys.* **62**, 1671 (1987).
- ¹⁰See, for example, M. H. Key, C. L. S. Lewis, and M. J. Lamb, *Opt. Commun.* **28**, 331 (1979).

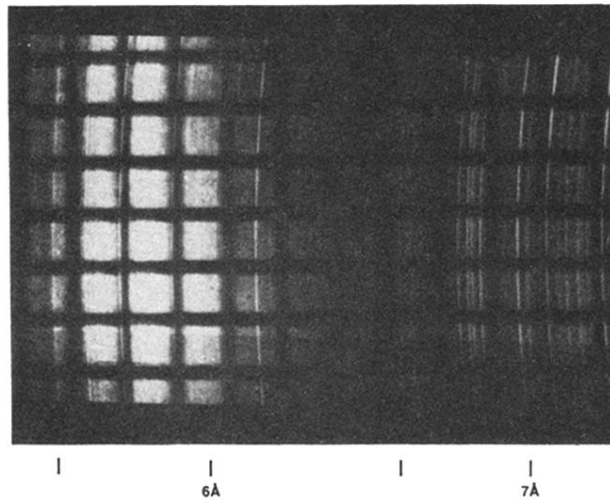


FIG. 2. Resolution grid showing the limitations on the spatial resolution due to source size and intensity. The source is a quasipoint tungsten pin. The grid has $30\text{-}\mu\text{m}$ -thick wires with a period of $120\text{ }\mu\text{m}$.

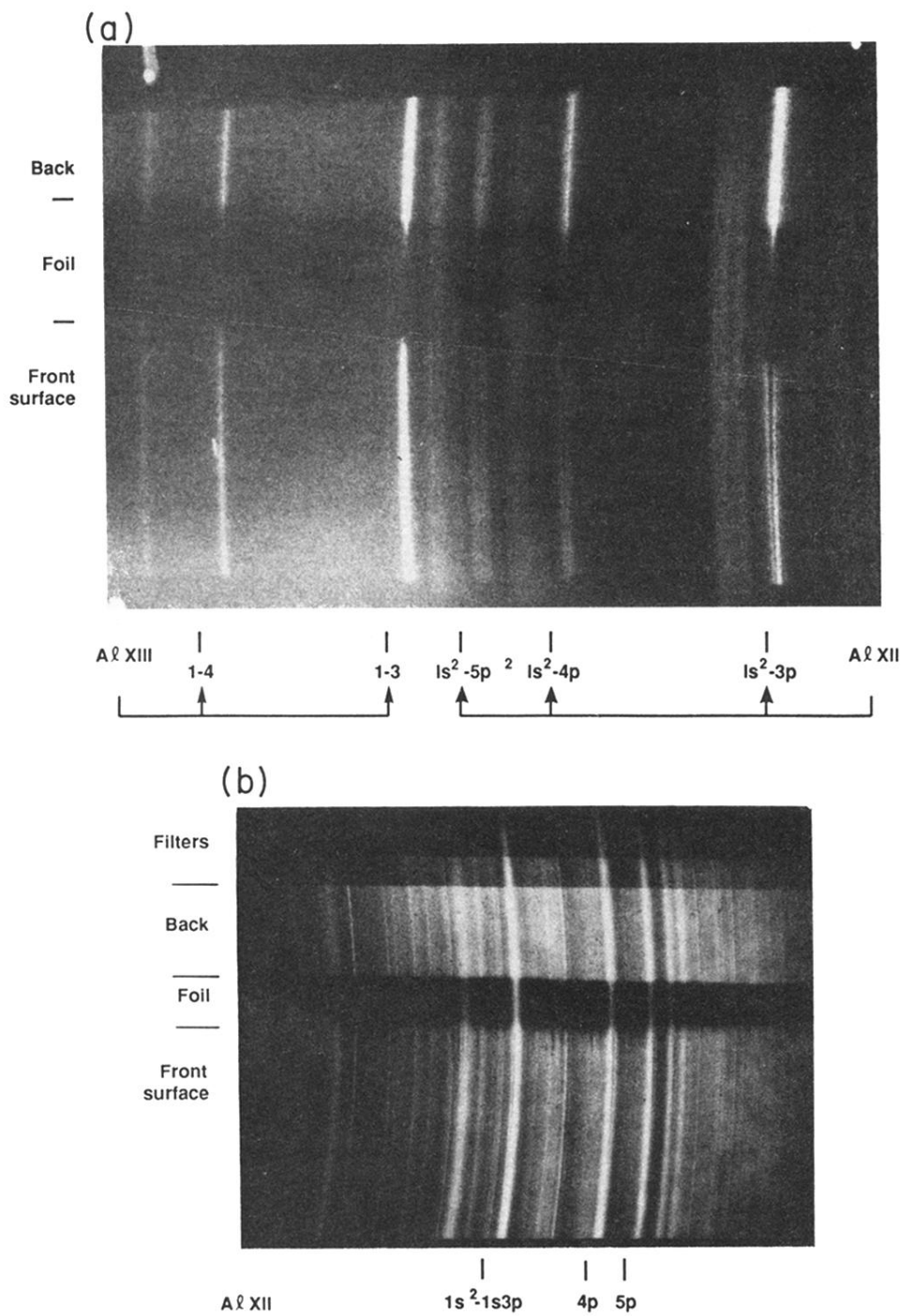


FIG. 3. (a) Data for an aluminum target backlit by an aluminum point source with a delay of 0 ps from the main pulse and a duration of 600 ps. (b) Data for an aluminum target backlit with a ytterbium point source with a delay of 0 ps from the main pulse and a duration of 100 ps.

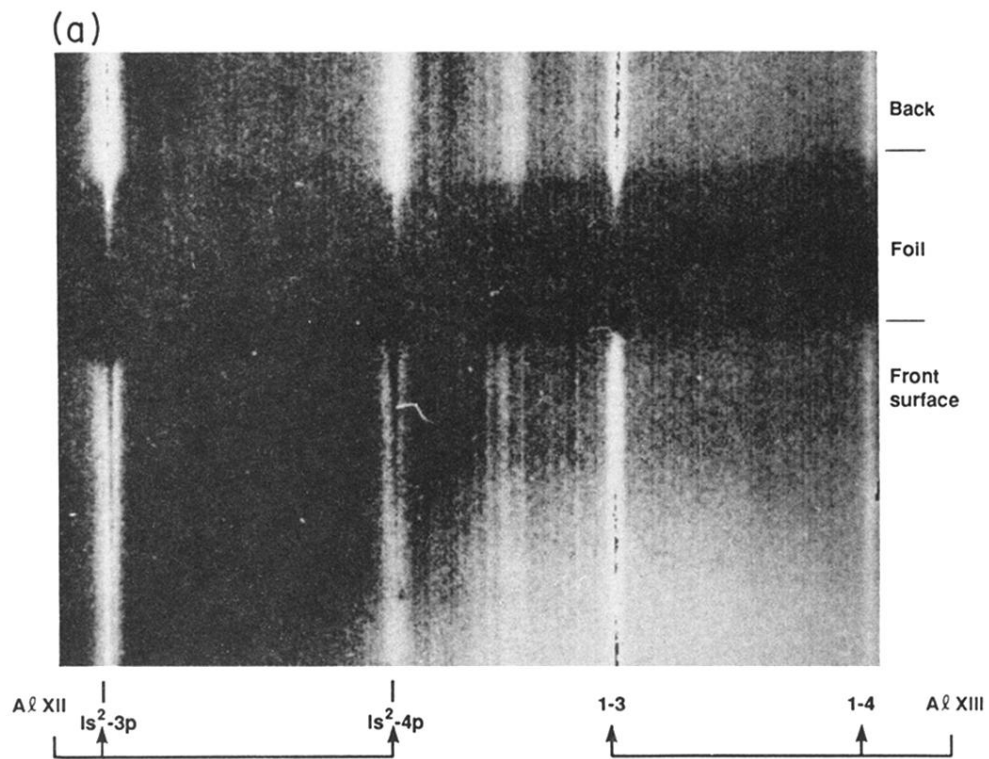


FIG. 4. (a) Processed data from shot illustrated in Fig. 3(a). (b) Processed data from an aluminum target backlit with a tungsten backlight of 600 ps in duration. Note that improved resolution is obtained with the broadband backlight source and that the complex structure of the backlight source is not a difficulty in the interpretation of the data.

(b)

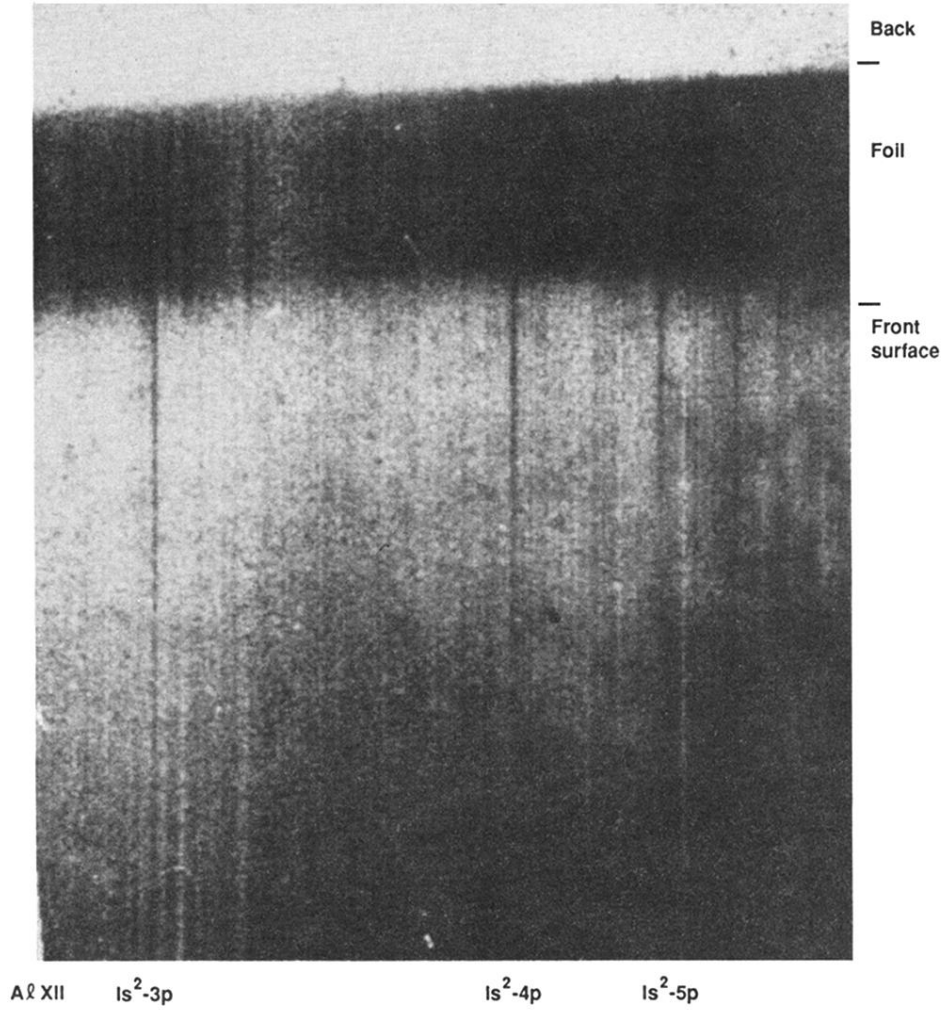


FIG. 4. (Continued).

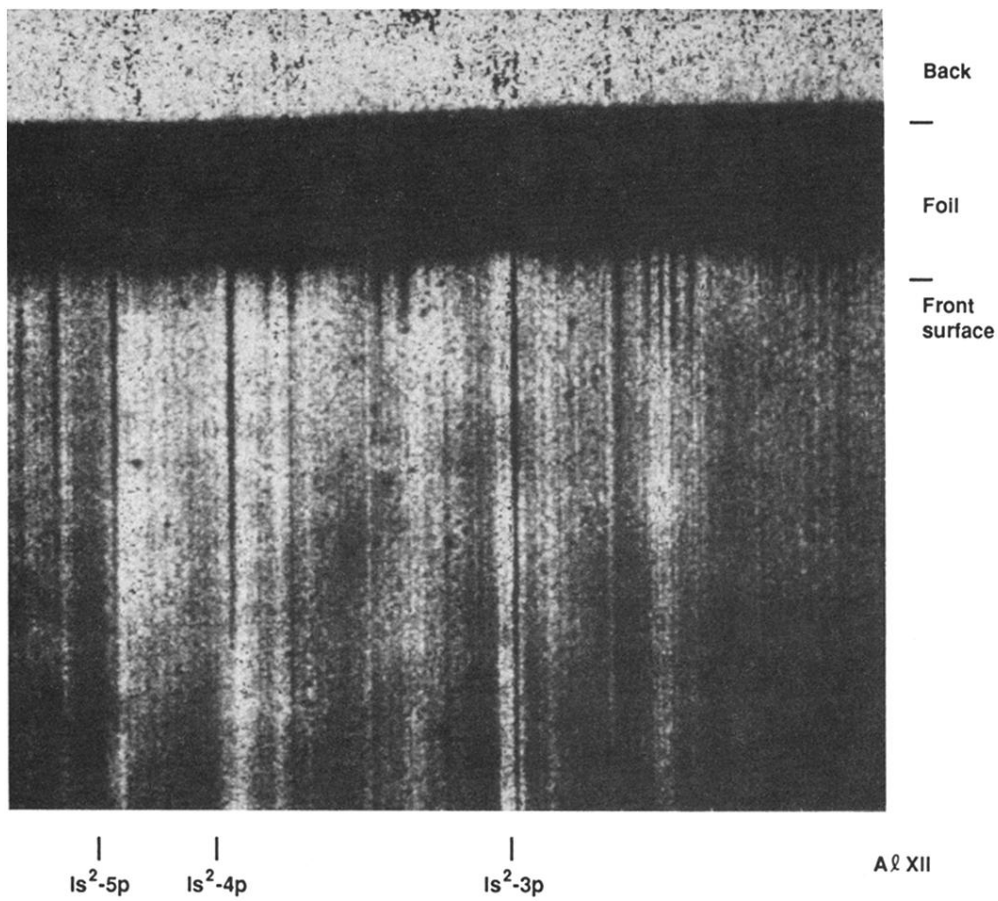


FIG. 5. Processed data from the experiment shown in Fig. 3(b).